Structural Engineering and Mechanics, *Vol. 66, No. 5 (2018) 583-594*
DOI: https://doi.org/10.12989/sem.2018.66.5.583

Stability and parameters influence study of fully balanced hoist vertical ship lift

Xionghao Cheng, Duanwei Shi*, Hongxiang Li, Re Xia, Yang Zhang and Ji Zhou

School of Power and Mechanical Engineering, Wuhan University, Wuhan 430072, China

(Received January 30, 2018, Revised March 4, 2018, Accepted March 5, 2018)

Abstract. A theoretical formulation based on the linearized potential theory, the Descartes' rule and the extremum optimization method is presented to calculate the critical distance of lifting points of the fully balanced hoist vertical ship lift, and to study pitching stability of the ship lift. The overturning torque of the ship chamber is proposed based on the Housner theory. A seven-free-degree dynamic model of the ship lift based on the Lagrange equation of the second kind is then established, including the ship chamber, the wire rope, the gravity counterweights and the liquid in the ship chamber. Subsequently, an eigenvalue equation is obtained with the coefficient matrix of the dynamic equations, and a key coefficient is analyzed by innovative use of the minimum optimization method for a stability criterion. Also, an extensive influence of the structural parameters contains the gravity counterweight wire rope stiffness, synchronous shaft stiffness, lifting height and hoists radius on the critical distance of lifting points is numerically analyzed. With the Runge-Kutta method, the four primary dynamical responses of the ship lift are investigated to demonstrate the accuracy/reliability of the result from the theoretical formulation. It is revealed that the critical distance of lifting points decreases with increasing the synchronous shaft stiffness, while increases with rising the other three structural parameters. Moreover, the theoretical formulation is more applicable than the previous criterions to design the layout of the fully balanced hoist vertical ship lift for the ensuring of the stability.

Keywords: fully balanced hoist vertical ship lift; stability; critical distance of lifting points; linearized potential theory; Descartes' rule; Runge-Kutta method

1. Introduction

In a full balanced hoist vertical ship lift, the ship chamber is housed in a long, narrow, rectangular tank. Liquid in this tank can lead to excessive inertia, weak bearing stiffness and ultimately poor dynamical characteristics of the ship lift. Therefore, it is of great significance of doing research on the stability of ship lift (Shi *et al.* 2015). Full balanced hoist vertical ship lifts combined with several sub-structures, such as gear retarder, synchronous shafts and gravity counterweights, are the main parts of mechanical-electric-hydraulic integrated complex systems. Liquid sloshing in the ship chamber can influence the system during raising and lowering of the ship chamber contributing to complicated dynamical characteristics in the full balanced hoist vertical ship lifts (Schinkel 2001, Michael 2014, Bai 2015, Liao *et al.* 2017).

Several magnetorheological isolation systems and control algorithms were proposed for suppressing the whipping effect of the ship lift towers (Qu *et al.* 2001, Tu *et al.* 2007, Qu *et al.* 2008). Subsequently, a fuzzy semi-active control strategy for seismic response reduction amid the wind load, using a magnetorheological damper (Zhou 2015). The coupled vibration between the ship lift and ship chamber was analyzed with the connection of the magnetorheological fluid damper for the better vibration damping effect (Zhong *et al.* 2016). The transient response of the system was analyzed by the Wilson-θ method, and the results verified the safety and reliability of the Three Georges ship lift design. A control equation of a coupling system was developed using a liquid dynamical equation by Li (2005). Liquid response, pitching motion of the ship chamber and motion of the ship can be analyzed by this control equation on condition of the earthquake.

Criteria for ship lift stability can be derived with static balanced and leakage condition (Chen 1996). Free vibration and stability of a full balanced hoist vertical ship lift, including the ship chamber, wire rope, gravity counterweights, liquid and ship were studied by Cheng (Li 2005, Ruan 2003) and the study identified critical factors affecting free vibration of the system and then figured out the critical distance of lifting points to maintain stability. The stability of free vibration for a ship chamber was analyzed by Shi (2003), a set of nonlinear differential equations containing eight variables were derived with potential flow theory of fluid mechanics and numerical simulation by the Runge-Kutta method and results found that the instability vibration of liquid in the ship chamber could emerge on the condition of emergency brake. A dynamical model of a full balanced hoist vertical ship lift was established by Liao (2014), based on the analysis of influential parameters of a synchronous shaft, a theoretical formulation to analyze critical distance of lifting points was developed without considering gravity counterweights.

The primary analytic methods in the field of engineering system stability analysis include the Routh-Hurwitz theory,

*Corresponding author, Professor
E-mail: 2016202080025@whu.edu.cn

ISSN: 1225-4568 (Print), 1598-6217 (Online)

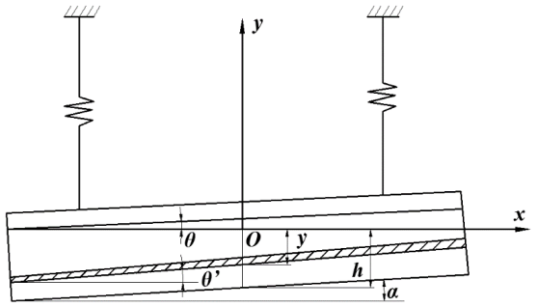

Fig. 1 Pitching motion diagram of ship chamber

Lyapunov theory, Floquet theory, and the Mathieu equation (Náprstek 2015). The Lyapunov theory is usually applied to linear and nonlinear systems. However, the establishment of the Lyapunov function is difficult, especially for the analysis of multi-free degree systems, time-variant systems and nonlinear systems (Ahmadian 1985, Doyle 1997). The Floquet theory and Mathieu equation are applicable for studying stability of linear homogeneous differential equations with periodic coefficients (Wimmer 1975, Weyh 1991, Ricci 2012). For linear systems with a constant coefficient, positive and negative roots of the characteristic equation can be evaluated using the Routh–Hurwitz theory. When the coefficient matrix of the differential equation set is transferred into the characteristic equation, stability of system can be analyzed according to the root of the characteristic equation (Song 2015, Schultz 1963, Tang 2013, Lancaster 1969). However, for an n orders characteristic equation where $(n+1)/2$ coefficient determinants are obtained by the Routh-Hurwitz theory, the maximum number of determinant is $(n+1)/2$. Thus, the calculation will be too complicated when it is utilized to analyze the multi-free degree systems.

Section 2 of this paper develops a dynamical model of a full balanced hoist vertical ship lift, including the ship chamber, wire rope, gravity counterweights, liquid, hoists and pulleys. Section 3 proposes a design formula to analyze critical distance of lifting points is derived using the Descartes' rule, which is further integrated with the Routh-Hurwitz theory to verify the results. Compared with previous research, this study provides a more complete dynamical model to avoid complicated results obtained by the Routh-Hurwitz theory simply. In Sec. 4, the dynamical simulation is used to analyze the primary displacement response of the system, and the stability of system is evaluated based on the convergence of displacement response. Finally, the results from the comparison of the simulation and the theoretical results are proved the validity of the theoretical formulation.

2. Description for dynamical modal

Fig. 1 signifies that the full balanced hoist vertical ship lift is in a suspended state and represents a pitching motion by angle acceleration $\ddot{\alpha}$ due to initial disturbance. The free surface of liquid in ship chamber is excited to make shaking vibration by angle acceleration $\ddot{\theta}$, and hydrodynamic pressure is generated to form overturning torque at the

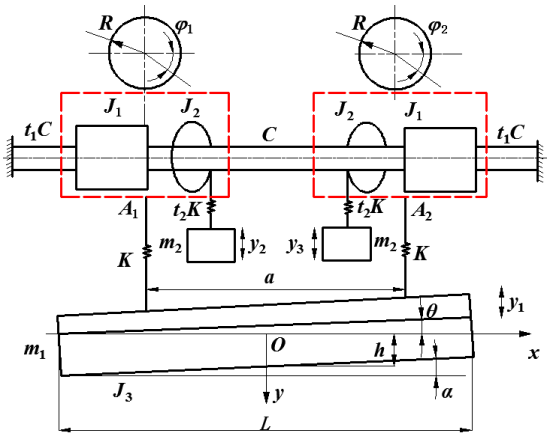

Fig. 2 Model diagram of the full balanced hoist vertical ship lift

bottom and end of the ship chamber. As the longitudinal length of the ship chamber is much than the height and width of the ship chamber, the overturning torque on the side wall of the ship chamber could be neglected to simplify the calculation system, and then the overturning torque formed by uneven distribution of the hydrodynamic pressure along the bottom of the ship chamber is calculated. There is a unit thickness layer (the shadow part in Fig. 1) at a liquid depth of y. According to the linearized potential theory, assuming incompressible, irrotational and inviscid fluid, the component v of the fluid velocity along the x direction should be satisfied

$$v = x\frac{\partial \theta'}{\partial t} \tag{1}$$

In Eq. (1), $\dot{\theta}'$ is the rotational angle velocity of the unit thickness layer at depth y. Based on Housner theory, θ and $\dot{\theta}'$ should satisfy the formula (Housner 1997)

$$\frac{\partial^2 \theta'}{\partial y^2} - \frac{10}{L^2}\frac{\partial \theta'}{\partial t} = 0 \tag{2.1}$$

$$\frac{\partial^2}{\partial t^2}\left(\frac{\partial \theta'}{\partial y}\right)_{y=0} + g\frac{10}{L^2}\theta = 0 \tag{2.2}$$

According to the actual situation, the boundary conditions could be as follows

$$\theta' = \theta, \frac{\partial \theta'}{\partial t} = \frac{\partial \theta}{\partial t}, \frac{\partial^2 \theta'}{\partial t^2} = \frac{\partial^2 \theta}{\partial t^2} (y = 0) \tag{3.1}$$

$$\theta' = \alpha, \frac{\partial \theta'}{\partial t} = \frac{\partial \alpha}{\partial t}, \frac{\partial^2 \theta'}{\partial t^2} = \frac{\partial^2 \alpha}{\partial t^2} (y = -h) \tag{3.2}$$

Based on Eqs. (2.1), (2.2) and Eqs. (3.1), (3.2), the relationship between θ and θ' is as follows

$$\theta' = \frac{\theta \cosh\sqrt{\frac{10}{L^2}}h - \alpha}{\sinh\sqrt{\frac{10}{L^2}}h} \sinh\sqrt{\frac{10}{L^2}}y + \theta\cosh\sqrt{\frac{10}{L^2}}y \tag{4.1}$$

$$\frac{\frac{\partial\theta}{\partial t}\cosh\sqrt{\frac{10}{L^2}}h-\frac{\partial\alpha}{\partial t}}{\sinh\sqrt{\frac{10}{L^2}}h}\sinh\sqrt{\frac{10}{L^2}}y+\frac{\partial\theta}{\partial t}\cosh\sqrt{\frac{10}{L^2}}y \tag{4.2}$$

Substituting Eqs. (4.1), (4.2) into Eqs. (2.1), (2.2), the relationship between α and θ is as follows

$$\ddot{\theta}+\frac{10gh}{L^2}\theta-\ddot{\alpha}=0 \tag{5}$$

P is the hydrodynamic pressure generated by the sloshing of the free surface of liquid in the ship chamber, and when y=0, P=0. By the Bernoulli equation, Eq. (1) and Eq. (5) are as follows

$$P=-\rho x\sqrt{\frac{L^2}{10}}\left[\frac{\ddot{\theta}\cosh\sqrt{\frac{10}{L^2}}h-\frac{\partial^2\alpha}{\partial t^2}}{\sinh\sqrt{\frac{10}{L^2}}h}\left(\cosh\sqrt{\frac{10}{L^2}}y-1\right)+\frac{\partial^2\theta}{\partial t^2}\sinh\sqrt{\frac{10}{L^2}}y\right] \tag{6}$$

When y=-h, due to $(\sqrt{10}h/L)\le 1$, so 1-cosh($\sqrt{10}h/L$)≈(-$5h^2/L^2$) and sinh($\sqrt{10}h/L$)≈($\sqrt{10}h/L$). The hydrodynamic pressure on the ship chamber can be as follows

$$P\approx\frac{1}{2}\rho xh\left(\frac{\partial^2\theta}{\partial t^2}+\frac{\partial^2\alpha}{\partial t^2}\right) \tag{7}$$

The overturning torque caused by hydrodynamic pressure is as follows

$$M_1=-\int_{-L/2}^{L/2}P_{y=-h}Bx\,dx=-J_s\left(\frac{\partial^2\theta}{\partial t^2}+\frac{\partial^2\alpha}{\partial t^2}\right) \tag{8}$$

where J_S=(1/24)ρBhL^3, and B is the width of the ship chamber. In addition, the overturning torque caused by the uneven liquid depth caused by the pitching of the ship chamber itself and sloshing of the free surface of liquid can be written as

$$M_2=-\int_{-L/2}^{L/2}\rho Bgx^2(\alpha-\theta)dx=\\=C_s(\alpha-\theta) \tag{9}$$

where C_S=(1/12)ρBhL^3 and g is acceleration of gravity.

Therefore, the total overturning torque of the ship chamber consisted of hydrodynamic pressure and hydrostatic pressure in two parts, it can be written as

$$M=M_1+M_2=-J_s(\ddot{\theta}+\ddot{\alpha})+C_s(\alpha-\theta) \tag{10}$$

A simplified dynamic model of a full balanced hoist vertical ship lift is shown in Fig. 2 and is in condition where the clamping equipment, the safety brake and the working brake have been released before the lifting of the ship chamber. P_1 and P_2 being two equivalent lifting points respectively, K being the stiffness of the wire rope for the ship chamber, C being the stiffness of synchronous shaft, R being the radius of the hoists and pulleys. The ship chamber is regarded as a rigid beam subjected to both hydrodynamic and hydrostatic pressure. Hence, the total kinetic energy and total potential energy of the system are as follows

$$T=\frac{1}{2}J_1(\dot{\varphi}_1^2+\dot{\varphi}_2^2)+\frac{1}{2}J_2(\dot{\varphi}_1^2+\dot{\varphi}_2^2)+\frac{1}{2}J_3\dot{\alpha}^2+\frac{1}{2}m_1\dot{y}_1^2+\frac{1}{2}m_2\dot{y}_2^2+\frac{1}{2}m_2\dot{y}_3^2 \tag{11.1}$$

$$V=\frac{1}{2}K\left(R\varphi_1-y_1-\frac{1}{2}a\alpha\right)^2+\frac{1}{2}K\left(R\varphi_2-y_1+\frac{1}{2}a\alpha\right)^2+\frac{1}{2}t_2K(R\varphi_1+y_2)^2+\frac{1}{2}C(\varphi_1-\varphi_2)^2+\frac{1}{2}t_1C(\varphi_1^2+\varphi_2^2)+\frac{1}{2}t_2K(R\varphi_2+y_3)^2 \tag{11.2}$$

where J_1 denotes the equivalent moment of inertia for the hoist and torque counterweights, with J_2 being the equivalent moment of inertia for the pulleys, J_3 being the equivalent moment of inertia for the pitching motion of the ship chamber and liquid, m_1 being the mass of liquid and ship chamber, m_2 being the mass of gravity counterweights. φ_1 being angle displacement of rotation for the hoists and pulleys in P_1, φ_2 being angle displacement of rotation for the hoists and pulleys in P_2, y_1 and y_2 being displacements along vertical direction of the gravity counterweights m_2 in upstream and downstream respectively, y_3 being displacement along vertical direction of ship chamber, α being angle displacement of pitching motion for the ship chamber, θ being angle displacement of sloshing for free surface of liquid.

With Lagrange equation of the second kind and taking damping into consideration, the differential equation of dynamics of the full balanced hoist vertical ship lift can be written as

$$(J_1+J_2)\ddot{\varphi}_1+\gamma_1\dot{\varphi}_1+KR(R\varphi_1-y_1-\frac{1}{2}a\alpha)+t_2KR(R\varphi_1+y_2)+C(\varphi_1-\varphi_2)+t_1C\varphi_1=0 \tag{12.1}$$

$$(J_1+J_2)\ddot{\varphi}_2+\gamma_1\dot{\varphi}_2+KR(R\varphi_2-y_1+\frac{1}{2}a\alpha)+t_2KR(R\varphi_2+y_3)-C(\varphi_1-\varphi_2)+t_1C\varphi_2=0 \tag{12.2}$$

$$(J_3+2J_s)\ddot{\alpha}+\gamma_2\dot{\alpha}-J_s\frac{10gh}{L^2}\theta-C_s(\alpha-\theta)-\frac{1}{2}aK(R\varphi_1-y_1-\frac{1}{2}a\alpha)+\frac{1}{2}aK(R\varphi_2-y_1+\frac{1}{2}a\alpha)=0 \tag{12.3}$$

$$(J_3+2J_s)\ddot{\theta}+\gamma_2\dot{\alpha}+(J_s+J_s)\frac{10gh}{L^2}\theta-C_s(\alpha-\theta)-\frac{1}{2}aK(R\varphi_1-y_1-\frac{1}{2}a\alpha)+\frac{1}{2}aK(R\varphi_2-y_1+\frac{1}{2}a\alpha)=0 \tag{12.4}$$

$$m_1\ddot{y}_1+\gamma_3\dot{y}_1-K(R\varphi_1-y_1-\frac{1}{2}a\alpha)-K(R\varphi_2-y_1+\frac{1}{2}a\alpha)=F \tag{12.5}$$

$$m_2\ddot{y}_2+\gamma_3\dot{y}_2+t_2K(R\varphi_1+y_2)=0 \tag{12.6}$$

$$m_2\ddot{y}_3+\gamma_3\dot{y}_3+t_2K(R\varphi_2+y_3)=0 \tag{12.7}$$

In the Eqs. (12), γ_i (i=1,2,3) respectively are the damping coefficient of the torsional vibration of the hoists and the pulleys, the damping coefficient of the pitching motion for ship chamber and the damping coefficient of the vertical motion for ship chamber. In the Eq. (12.5), F is a dynamic load caused by the hydrodynamic pressure and the hydrostatic pressure on the bottom of the ship chamber in the vertical direction

$$F = \int_{-L/2}^{L/2} BP_{y=-h}dx + \int_{-L/2}^{L/2} \rho gB[h-(\alpha-\theta)x]dx - \int_{-L/2}^{L/2} \rho gBhdx \tag{13}$$

substituting Eq. (7) into Eq. (13), $F=0$ is obtained. The dynamic equations of the system can be collated as follows

$$\frac{\partial \boldsymbol{X}}{\partial t} = A\boldsymbol{X} = \begin{bmatrix} A_{11} & A_{12} \\ A_{21} & A_{22} \end{bmatrix} \boldsymbol{X} \tag{14}$$

In the Eq. (14), A_{ij} (i=1,2; j=1,2) is a matrix of 7×7, with its detailed expression are organized into Appendix A. $\boldsymbol{X}$ and $\dot{\boldsymbol{X}}$ are the matrix of 8×1, they are written as follows

$$\boldsymbol{X}^T = \left[\frac{\partial \varphi_1}{\partial t} \quad \varphi_1 \quad \frac{\partial \varphi_2}{\partial t} \quad \varphi_2 \quad \frac{\partial \alpha}{\partial t} \quad \alpha \quad \frac{\partial \theta}{\partial t} \quad \theta \quad \frac{\partial y_1}{\partial t} \quad y_1 \quad \frac{\partial y_2}{\partial t} \quad y_2 \quad \frac{\partial y_3}{\partial t} \quad y_3 \right]^T \tag{15}$$

3. Stability analysis for dynamical modal

3.1 Critical distance formulation

The eigenvalue equation of matrix A in Eq. (15) can be written as follows

$$\sum_{i=0}^{14} b_i r^{14-i} = 0 \tag{16}$$

where b_i (i=0,1,2,⋯,14) can be calculated using Eq. (15) and Eq. (16). For algebraic equations of real coefficients with one-factor n orders, such as Eq. (16), a coefficient sequence can be as follows

$$T = \{b_0, b_1, \cdots, b_{14}\} \tag{17}$$

According to the Descartes' rule, the symbols of two contiguous coefficient b_k, b_{k+1} (k=0,1,2,⋯,13) in Eq. (17) are opposite and should be defined as symbol change. With an assumption of the times for symbol change with coefficient sequence T is p, Eq. (16) has no positive root if p=0, and the system is stable. From Eq. (14) and Eq. (16), b_i (i=0,1,2,⋯,14) can be obtained in Appendix B. For p=0, b_i (i=1,2,3,⋯,14) are greater than zero constantly because of b_0=1>0. Subsequently, on the basis of the universal design criteria for the ship lift, the range of the primary parameters K, R, C, J_1, J_2, J_3 and J_S should be of 10^6-10^{11} magnitude,

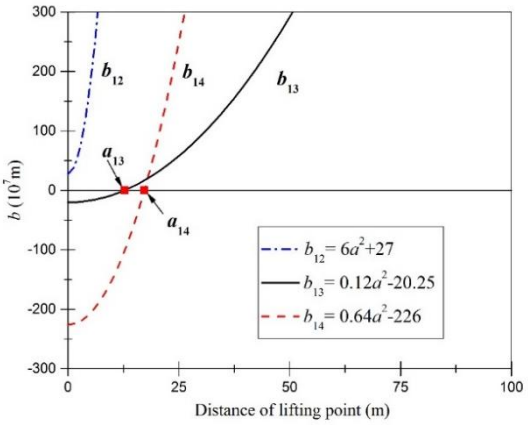

Fig. 3 Function curve shape for b_i (i=12,13,14)

the minimums of each coefficient b_i (i=10,11,12⋯,14) can be obtained by the extremum optimization method respectively in the change of a∈[0, 200] (there is no possibility of exceeding 200 for the distance of the lifting points in the ship lift), based on Eqs. (B.11), (B.12), (B.13), (B.14), (B.15) with the corresponding value is min[b_i (i=10,11,12⋯,14)]=[63, 57, 22, -45, -258]. Owing to the quadratic function with an argument for b_i (i=0,1,2⋯,14), b_{14} is greater than zero constantly for the lowest minimum among coefficients b_i (i=10,11,12 ⋯ ,14), and other coefficients have the eternal upper zero values. Ultimately, a_{cr}, the critical distance of the lifting points when b_{14}=0, is as follows by constituting Eqs. (A.7)-(A.25) into b_{14}

$$a_{cr} = \sqrt{\frac{2C_s[(A_1-A_2)B_1+B_3]}{K(1+t_2)[(A_1-A_2)B_1+B_3]+(A_1-A_2)B_2}} \tag{18}$$

where A_i (i=1, 2), B_i (i=1, 2, 3) can be calculated as follows

$$A_1 = \left[(J_3+2J_s)\frac{10gh}{L^2} + C_s \right] [KR^2(1+t_2)+(1+t_1)C] \tag{19.1}$$

$$A_2 = \left(C_s - J_s\frac{10gh}{L^2} \right) [KR^2(1+t_2)+(1+t_1)C] \tag{19.2}$$

$$B_1 = (1+t_1)C - t_2KR^2 \tag{19.3}$$

$$B_2 = K^2R^2(t_2^2-1) - t_2KC(1+t_1) - \frac{(1+t_2)t_2^2K^3R^4}{[KR^2(1+t_2)+(1+t_1)C]} \tag{19.4}$$

$$B_3 = t_2^2K^2R^4\left(3J_s\frac{10gh}{L^2} + J_3\frac{10gh}{L^2} \right) \tag{19.5}$$

To illustrate the use of Eq. (18), for the full balanced hoist vertical ship lift, the second step of the GouPitan ship lift, because of the greatest lifting height and lifting mass (H=113 m, m_1=m_2=1075 t) throughout China, is used for a sample calculation. The primary parameters include J_1=1.05×10^7 kg·m^2, J_2=1.05×10^7 kg·m^2, J_3=9.2×10^8 kg·m^2, C_S=4.77×10^9 kg·m^2, J_S=5.97×10^8 kg·m^2, L=71 m, h=2.5 m,

t_1=2, t_2=4, K=3.0×10^{7}N/m, C=1.5×10^9 N/m, t_1=2, and t_2=4, are constituted into Eq. (16) and Eq. (18). Therefore, the function curve of b_i (i=12,13,14) is shown in Fig. 3 with $a\in$ [0, 30] (b_{12}=6a^2+27, b_{13}=0.12a^2-20.25, b_{14}=0.64a^2-226), and the lowest minimum of three coefficients is between -300 and -200 in b_{14}. So, a_{cr}=18.73 m (Table 1).

Now, by constituting the parameters of the second step of GouPitan ship lift into Eq. (16), the eigenvalue equation can be written as follows

$$\begin{aligned}\sum_{i=0}^{14} b_i r^{14-i} &= r^{14}+9r^{13}+780r^{12}+5400r^{11}\\ &+(0.02r^{10}+0.1r^9+2.4r^8+7r^7+110r^6\\ &+160r^5+1500r^4+1000r^3+4600r^2\\ &+2500r+5400)\times 10^7\end{aligned} \tag{20}$$

Next, on base of the Routh-Hurwitz theory (Lancaster 1969), b_i (i=0,1,2, ⋯,14) should be satisfied with the necessary and sufficient conditions as follows

$$\Delta_{2n-1}=\begin{bmatrix} b_1 & b_3 & \cdots & b_{2k-1} & \cdots & 0\\ b_0 & b_2 & \cdots & b_{2k-2} & \cdots & 0\\ 0 & b_1 & \cdots & b_{2k-3} & \cdots & 0\\ \vdots & \vdots & \cdots & \vdots & \vdots & \vdots\\ 0 & 0 & \cdots & 0 & \cdots & b_{2n-1}\end{bmatrix} \tag{21}$$

where n, k=(1,2,3,⋯,7), $n\geq k$. Then, the results are calculated as follows

$$\Delta_1=b_1=9.4>0 \tag{22.1}$$

$$\Delta_3=\begin{bmatrix} b_1 & b_3 & b_5\\ b_0 & b_2 & b_4\\ 0 & b_1 & b_3\end{bmatrix}=1.5\times 10^6>0 \tag{22.2}$$

$$\Delta_5=\begin{bmatrix} b_1 & b_3 & b_5 & b_7 & b_9\\ b_0 & b_2 & b_4 & b_6 & b_8\\ 0 & b_1 & b_3 & b_5 & b_7\\ 0 & b_0 & b_2 & b_4 & b_6\\ 0 & 0 & b_1 & b_3 & b_5\end{bmatrix}=2.5\times 10^{15}>0 \tag{22.3}$$

$$\Delta_7=\begin{bmatrix} b_1 & b_3 & b_5 & \cdots & b_{13}\\ b_0 & b_2 & b_4 & \cdots & b_{12}\\ 0 & b_1 & b_3 & \cdots & b_{11}\\ \vdots & \vdots & \vdots & \vdots & \vdots\\ 0 & 0 & b_1 & \cdots & b_7\end{bmatrix}=1.0\times 10^{28}>0 \tag{22.4}$$

$$\Delta_9=\begin{bmatrix} b_1 & b_3 & b_5 & \cdots & 0\\ b_0 & b_2 & b_4 & \cdots & 0\\ 0 & b_1 & b_3 & \cdots & 0\\ \vdots & \vdots & \vdots & \vdots & \vdots\\ 0 & 0 & 0 & \cdots & b_9\end{bmatrix}=6.1\times 10^{44}>0 \tag{22.5}$$

$$\Delta_{11}=\begin{bmatrix} b_1 & b_3 & b_5 & \cdots & 0\\ b_0 & b_2 & b_4 & \cdots & 0\\ 0 & b_1 & b_3 & \cdots & 0\\ \vdots & \vdots & \vdots & \vdots & \vdots\\ 0 & 0 & 0 & \cdots & b_{11}\end{bmatrix}=8.9\times 10^{63}>0 \tag{22.6}$$

$$\Delta_{13}=\begin{bmatrix} b_1 & b_3 & b_5 & \cdots & 0\\ b_0 & b_2 & b_4 & \cdots & 0\\ 0 & b_1 & b_3 & \cdots & 0\\ \vdots & \vdots & \vdots & \vdots & \vdots\\ 0 & 0 & 0 & \cdots & b_{13}\end{bmatrix}=2.6\times 10^{84}>0 \tag{22.7}$$

It can be seen from Eqs. (22.1)-(22.6) that Δ_{2n-1} (n=1,2,⋯,7) >0 proving that the critical distance of lifting points a_{14} satisfies the condition of system stability.

3.2 Influence for *gravity counterweights wire ropes*

Letting t_2=0 in Eq. (18), an equation can be obtained as follows

$$a' = \sqrt{\frac{1}{1-\dfrac{KR^2}{(1+t_1)C}}}\sqrt{\frac{2C_S}{K}} \tag{23}$$

Eq. (23) is a design formula to analyze the critical distance of lifting points neglecting the influence of synchronous shaft. Coefficient η is defined as η=(a/a'), for simplifying the analysis, stiffness of the motor driveshaft is neglected (t_2=0). Based on Eq. (18), η can be calculated as follows

$$\eta=\sqrt{\frac{C\left[C^2-K^2R^4(t_2+1)\right]+t_2K^3R^6}{C\left[C^2-K^2R^4(1+t_2)^2\right]}} \tag{24}$$

$$\begin{aligned}\frac{d\eta}{dt_2}&=\frac{K^4R^8t_2^2(KR^2-C)+2CK^2R^4t_2(2C^2-K^2R^4)}{C\left(C^2-K^2R^4(1+t_2)^2\right)^2}\\ &+\frac{K^2R^4\left(C^3+C^2R^2K-CK^2R^4-K^3R^6\right)}{C\left(C^2-K^2R^4(1+t_2)^2\right)^2}\end{aligned} \tag{25}$$

Let $d\eta/dt_2$ =0, the two zero points of Eq. (26) can be calculated as

$$t_2'=\pm\left[\frac{\left(4C^3-2CK^2R^4\right)}{2K^2R^4(KR^2-C)}+\frac{\sqrt{\left(4C^3-2CK^2R^4\right)^2-4KR^4(KR^2-C)\left(C^3+KC^2R^2-CK^2R^4-K^3R^6\right)}}{2K^2R^4(KR^2-C)}\right] \tag{26}$$

where t_2' represents the two extreme points of the coefficient η. The maximum of t_2' among seven most representative full balanced hoist vertical ship lifts in China, including the second step of the GouPitan ship lift, the GaoBazhou ship lift, the PengShui ship lift, the ShuiKou ship lift, the TingZikou ship lift, the first step of the GeHeyan ship lift and the second step of the GeHeyan ship lift, is 314 (the ShuiKou ship lift), the result is far beyond the normal engineering design range. Thus, η increases when t_2 increases in practical design of ship lift. Fig. 4 shows the variation law for η with the parameter t_2, based on Eq. (26). When the gravity counterweights wire ropes stiffness is relatively larger, the acceleration produced by m_1 and m_2 along vertical direction at the two lifting points present a greater degree, leading directly to greater rotation angle acceleration of the hoists and pulleys, and enhanced system stability. Moreover, the larger tension difference of gravity counterweights m_1 and m_2 at the two lifting points is caused by greater lifting height when the gravity counterweights wire ropes stiffness is larger, producing a

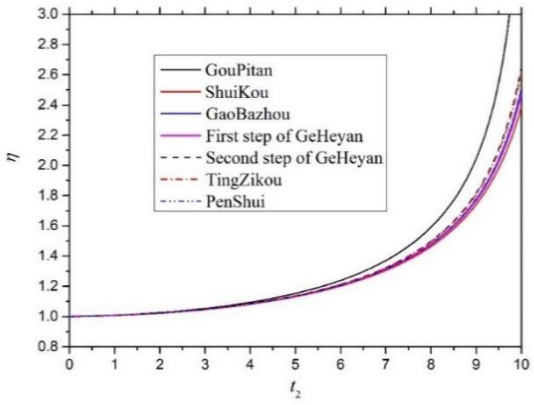

Fig. 4 Change for critical distance of lifting points with gravity counterweights wire ropes stiffness

larger angle acceleration of synchronous shaft caused torque difference at the hoists, contributing to the instability remarkably. Hence, as shown in Fig. 4, η shows an increasing trend with increasing t_2 when $0 \le t_2 \le 10$. When $t_2 > 5$, the influence of t_2 becomes more significant.

3.3 Influence of synchronous shaft

To simplify the calculating system, the relatively minimal-impact parameters such as gravity counterweights, synchronous shaft stiffness and angle displacement of free sloshing of liquid surface θ are neglected. Letting $\theta=0$, $\ddot{\theta}=0$ and $\ddot{\alpha}=0$ in Eq. (10), overturning torque caused by uneven distribution of hydrostatic pressure along the ship chamber is as follows

$$M' = C_s \alpha \tag{27}$$

In Fig. 2, anti-overturning torque caused by tension difference of wire rope at the two lifting points can be written as

$$M'' = \frac{1}{2} a_2^2 K \alpha \tag{28}$$

Assuming the side opposite to the ship chamber of the wire rope is fixed on the stander, the relationship between Eq. (27) and Eq. (28) is as $M'=M''$ with the static balanced condition (Liao 2014). Thus, it can be known from Eq. (28), Eq. (28) that revised formula should be as follows

$$a'' = \sqrt{\frac{2C_s}{K}} \tag{29}$$

Now, n indicates the safety tolerance of current design, a_0 shows the practical distance of lifting points, and a coefficient n can be defined as $n=(a_0/a)$. The similar construction of Eq. (23) and Eq. (29) in other study (Liao 2014). Therefore, for the validation of Eq. (18), Table 1 summarizes the results of Eq. (18), Eq. (23) and Eq. (29) for the seven most representative full balanced hoist vertical ship lifts in China. Here, the greatest error between a_{cr} and a' is 3.47% while 5.22% between a_{cr} and a'', and the maximum of n is 4.4 in the first step of GeHeyan ship lift,

Table 1 Results of for critical distance of lifting points of seven most representative full balanced hoist vertical ship lift in China

Ship lift names	Parameters				
	a_0	a_{cr}	a'	a''	n
The second step of GouPitan ship lift	36.2	18.73	18.09	17.83	1.93
GaoBazhou ship lift	26	5.77	5.57	5.49	4.51
PengShui ship lift	36	13.41	12.95	12.76	2.68
ShuiKou ship lift	75	31.02	29.96	29.52	2.42
TingZikou ship lift	60.05	37.43	36.15	35.63	1.60
The first step of GeHeyan ship lift	23.6	5.36	5.18	5.08	4.4
The second step of GeHeyan ship lift	24	5.40	5.22	5.14	3.2

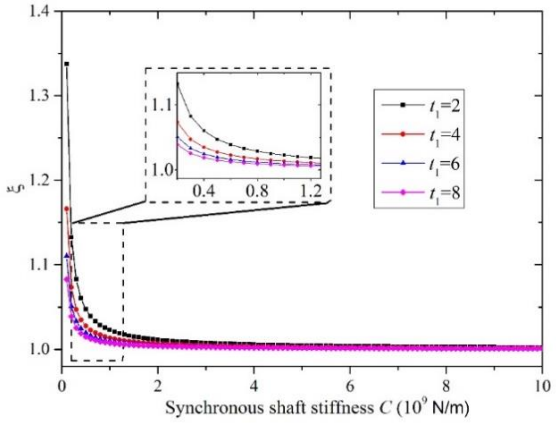

Fig. 5 Influence of synchronous shaft stiffness on the critical distance of lifting points

these demonstrate the application and accuracy/reliability of Eq. (18).

ξ, an influential coefficient of the synchronous stiffness on the critical distance of the lifting points, can be defined as $\xi=(a'/a'')$. By combining Eq. (23) with Eq. (29), ξ can be obtained as

$$\xi = \sqrt{\frac{1}{1-\dfrac{KR^2}{(1+t_1)C}}} \tag{30}$$

$$\frac{\partial \xi}{\partial C} = -\frac{KR^2\left[\dfrac{1}{1-\dfrac{KR^2}{C(1+t_1)}}\right]^{3/2}}{2C^2(1+t_1)} \tag{31}$$

The influence of lifting height on the critical distance of lifting points and synchronous shaft stiffness is shown in Fig. 5. The torque difference of the two hoists drop under the constrain of the synchronous shaft, contributing to the prevention of pitching for the ship chamber. Therefore, the critical distance of lifting points decreases with increasing synchronous shaft stiffness when t_1 is constant. However, the excessive synchronous stiffness causes the fixing approximation of the side for the ship chamber wire rope

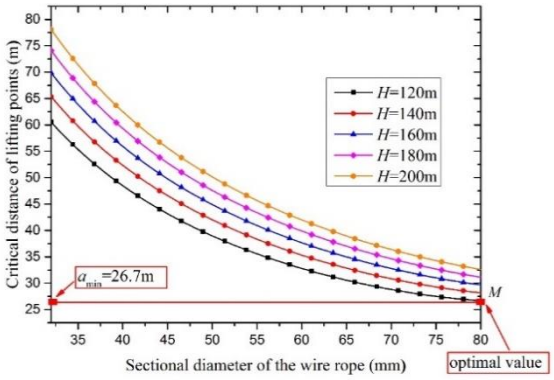

Fig. 6 Influence of lifting height on the critical distance of lifting points and sectional diameter of the wire rope

similar to the condition of Eq. (29), leading to a less obvious change of the critical distance of lifting points emerges with ξ approaching 1 in Fig. 5 when C exceeding 2×10^9 N/m. Also, the greater torque on the hoists caused by the greater stiffness differences of motor drive shaft and synchronous shaft, producing the excessive angle acceleration on the hoists and pulleys, enhancing the instability for the ship lift. Hence, the critical distance of lifting points decreases with increasing $t_1$when C keep constant.

3.4 Influence of lifting height

The stiffness of wire rope for a ship lift can be defined as

$$K = \frac{E\pi\left(\frac{d}{2}\right)^2}{H}N \tag{32}$$

where N is the total number of wire ropes for the ship lift, in this equation, n is set as 48; E is the elastic modulus of wire rope for the ship lift, let E=4.91×10^{10} N/m^2; and d is the sectional diameter of wire rope for the ship lift. The size of the hoists varies with the sectional area of the wire rope, and for vertical ship lift, sectional diameter of hoists D=2R=66d. Thus, combining Eq. (18) and Eq. (32), a function where critical distance of lifting points a varies with lifting height H and sectional diameter of wire rope d can be obtained as

$$a = \text{function}(H, d) \tag{33}$$

For guaranteeing enough safety tolerance n when H>120 m, it is necessary to make a minimum under the certain constraint condition. An increasing sectional area of the wire rope is presented with the higher lifting height of ship lift, avoiding the larger wire rope elasticity. Besides, the lifting weight of the ShuiKou ship lift is 500 t, meeting the operation condition when H>120 m. Thus, using the ShuiKou ship lift as an example, the constraint condition is defined as 32 mm<d<80 mm, 120m<H<200 m. Eq. (33) is optimized by the Lagrange multiplier method. Meeting the constraint conditions, it is calculated that a_{min}=26.7 m when

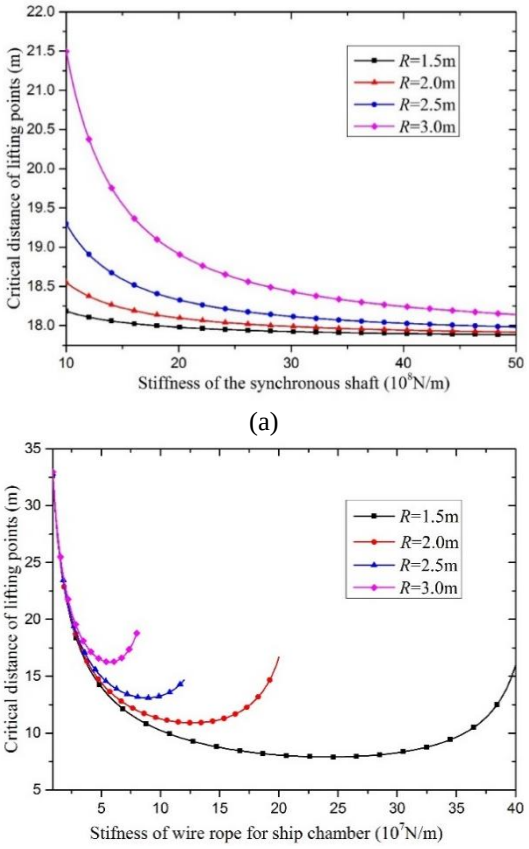

Fig. 7(a) Influence of the stiffness of the synchronous shaft on the critical distance of lifting points, (b) influence of the stiffness of the wire rope for the ship chamber on the critical distance of lifting points

H=120 m and d=80 mm. The improving system stability is guaranteed with relative lower lifting height and larger sectional area of wire rope.

The influence of lifting height on the critical distance of lifting points and sectional area of the wire rope is shown in Fig. 6. Based on the optimal results, M is the smallest critical distance of lifting points. The higher lifting height and smaller sectional diameter of the wire rope resulted to increasing elasticity, the weaker resistance to overturning capacity, enhancing instability of the system and increasing the critical distance of lifting points. Thus, the critical distance of lifting points presents an increasing trend related to the larger lifting height with constant sectional area, and the critical distance of lifting points increases with decreasing sectional area of the wire rope when the lifting height is constant.

3.5 Influence for hoists radius

The influence of the hoist radius on the synchronous shaft stiffness, wire rope stiffness and critical distance of the lifting points is shown in Fig. 7. An increasing hoists radius is attributed to a larger critical distance of lifting points when the synchronous shaft stiffness is constant. The increasing synchronous shaft stiffness is mainly due to the larger hoists radius when the critical distance of lifting

points is constant. The increasing synchronous shaft stiffness is caused by the reduction of critical distance of lifting points, and a larger influence is observed with increasing radius for hoists when $C < 3\times10^9$ N/m.

The hoists radius exert relatively little influence on the critical distance of lifting points when $K < 5\times10^7$ N/m. A larger critical distance of lifting points is observed with increasing hoists radius when $K > 5\times10^7$ N/m. With the increasing stiffness of the ship chamber's wire rope, the critical distance of lifting points firstly decreases, then increases after reaching the minimum value when the hoist radius is constant. The condition when the critical distance of lifting points reaches a minimum is defined as the optimal stability state. The larger hoists radius is related to decreasing stiffness of the ship chamber's wire rope, and the greater critical distance of lifting points increases at the optimal stability state.

When the wire rope's stiffness is too small, the anti-overturning torque caused by this wire rope is found to present a decreasing trend. The difference between the overturning torque and the anti-overturning torque increases largely, leading to a greater pitching angle acceleration of the ship chamber, and weaker system stability as the system takes a relatively long time to reach final steady state. When the wire rope's stiffness is too large, the anti-overturning torque causes this of wire rope increases. Larger difference between the overturning torque and the anti-overturning torque is observed, leading to a greater instantaneous pitching angle acceleration of the ship chamber due to the rapid recovery of the elastic deformation for the wire rope, weakening the system stability.

4. Dynamical simulation

Taking the second step of GouPitan ship lift as a simulation example, the angle displacement responses are calculated for the full balanced hoist vertical ship lift with the varying step four order Runge-Kutta method. The various angle displacements in the initial condition are taken as $\varphi_{10}=0$, $\varphi_{20}=0$, $\alpha_0=0.24°$, $\theta_0=0.2°$, and the simulation time is 500 s. When a=17.17 m or 17.18 m, the angle displacements are shown in Fig. 8. When a=17.17 m, all angle displacements diverge; when a=17.18 m, all angle displacements converge gradually to zero, and the full balanced hoist vertical ship lift are stable. Hence, a=17.18m is the critical distance of lifting points of the full balanced hoist vertical ship lift.

When a=17.18 m, compared with other angle displacements, the larger overturning torque of the ship chamber results to a maximum response for α after a period of time. Angle displacement of the sloshing free liquid surface θ is sensitive to the influence of the damping and the time for θ reaching stability (displacement response decays to zero) is the shortest accordingly. When the initial pitching motion of the ship chamber happens, due to the elastic deformation of the wire rope, the wire rope at the one of lifting points extend, and the other, however, shorten. Therefore, the rotation angle displacement of the hoists at the lifting points φ_1 and φ_2 are opposite in direction before

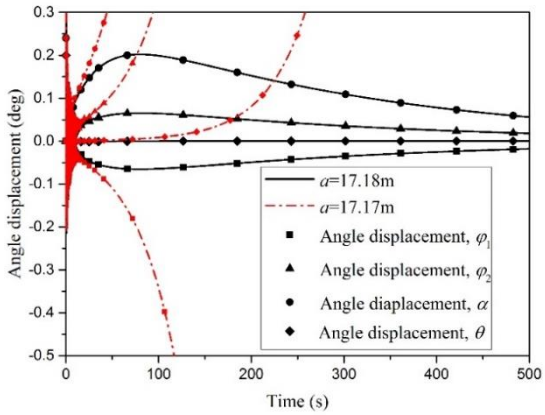

Fig. 8 Angle displacement responses of φ_1, φ_2, α and θ with damping

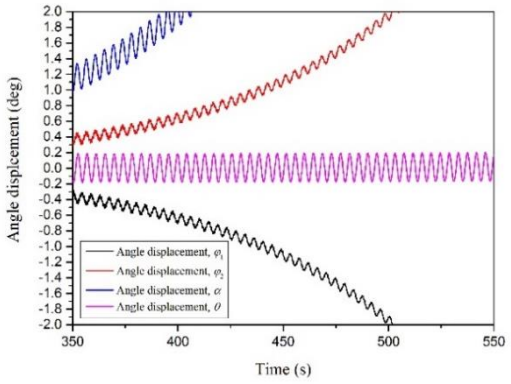

(a)

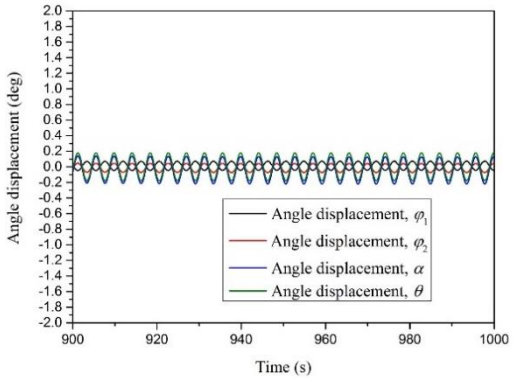

(b)

Fig. 9(a) Angle displacement responses of φ_1, φ_2, α and θ without damping when a=17.13 m, (b) Angle displacement responses of φ_1, φ_2, α and θ without damping when a=17.14 m

recovering to the initial state of no elastic deformation. Similarly, when a=17.17 m, α begins to diverge firstly, φ_1 and φ_2 are opposite, and diverge velocity of θ is the slowest.

In the Eq. (12.1)-(12.7), let γ_i (i=1,2,3)=0, the dynamic differential equations without damping are obtained, and the angle displacement responses are calculated by dynamical simulation. When a=17.13 m and 17.14 m respectively, the angle displacement responses are shown in Fig. 9. When a=17.13 m, the angle displacement responses are in divergence state, θ cannot diverge until time is close

to 850 s. However, when a is set as 17.14 m, the angle displacement responses converge gradually to zero, with reaching stable state finally. When a=17.14 m, the large displacement response is observed with α and θ, because of the larger external load of the ship chamber on condition of neglecting the influence of damping. The results present that the alternate change of the overturning torque could influence α trend largely.

The results of the critical distance of lifting points calculated by Eq. (18) are compared with the two opposite conditions: damping and no damping dynamical, and the according errors are calculated to be 9.02% and 9.30%, respectively. Thus, the correctness of the theoretical design formula is verified within the allowable range of engineering errors.

5. Conclusions

A rigorous theoretical formulation founded on the linearized potential theory, the Descartes' rule and the extremum optimization method for the stability criterion to investigate the critical distance of the lifting points. The dynamical model of the full balanced hoist vertical ship lift is more complete in comparison to the other works (Liao 2014), and the analysis of the effects from the primary four parameters on the critical distance of the lifting points are spelled out. The dynamical simulation demonstrates the accuracy/reliability of the consequences from the theoretical formulation. The key observations are summarized as follows:

• A theoretical formulation for the critical distance of lifting points is presented. The formulation could provide an academic reference for the practical layout and design of the full balanced hoist vertical ship lift includes hoists and pulleys, the gravity counterweights, the synchronous shafts, the wire rope and the ship chamber.

• Based on the results of the formulation, increasing the gravity counterweights wire ropes stiffness may result to the larger critical distance of lifting points amid the normal engineering design, with specific parameter t_2 in the range between 0 and 10. Also, the critical distance of the lifting points decreases and the drop tendency becomes slighter progressively with increasing the synchronous shaft stiffness.

• For the design of the full balanced hoist vertical ship lift with lifting height H higher than 120 m, the sectional diameter of the wire rope should be set to be larger to guarantee the adequate stiffness of wire rope.

• When the synchronous shaft stiffness C is larger than the critical value of 3×10^9 N/m, the influence of the radius of the hoists and pulleys on the critical distance of lifting points is greater. However, if the stiffness of the wire rope for ship chamber K is smaller than 5×10^7 N/m, the influence of the radius of the hoists on the critical distance of lifting points is relatively smaller. Therefore, it is important to obey the design principle that a lower stiffness of the wire rope for the ship chamber, and a greater stiffness of the synchronous shaft should be ensured. Without modifying other conditions, a moderate stiffness of the wire rope in the ship chambers should be maintained (i.e., when 1.5 m$\leq R\leq$3.0 m, K should be maintained at 5×10^7-9×10^7 N/m).

• Based on the four primary displacement response results of the ship lift, the larger response of angle displacement of the pitching motion for the ship chamber, the longer time required to reach final steady state. Therefore, the excessive initial pitching angles should be avoided during the operation of the full balanced hoist vertical ship lifts and the locking devices would be useful to maintain reliability.

Acknowledgments

The present work is carried out with the support of National Major Project Foundation of China (No.2016YFC0402002).

References

Ahmadian, M. and Inman, D.J. (1985), "On the stability of general dynamic systems using a Lyapunov's direct method approach", *Comput. Struct.*, **20**, 287-292.

Bai, W., Liu, X. and Koh, C.G. (2015), "Numerical study of violent LNG sloshing induced by realistic ship motions using level set method", *Ocean Eng.*, **97**, 100-113.

Chen, J.Z. and Ma, G.Y. (1996), "Chamber stability of hoisting fully balancing type vertical ship lift", *Hydro-Sci. Eng.*, **4**, 301-308.

Doyle, M.M., Sri Namachchivaya, N. and Van Roessel, H.J. (1997), "Asymptotic stability of structural systems based on Lyapunov exponents and torque Lyapunov exponents", *Int. J. Non-Lin. Mech.*, **32**(4), 681-692.

Housner, G., Bergman, L.A., Caughey, T.K., Chassiakos, A.G., Claus, R.O., Masri, S.F., Skelton, R.E., Soong, T.T., Spencer, B.F. and Yao, J.T. (1997), "Structural control: Past, present, and future", *J. Eng. Mech.*, **123**(9), 897-971.

Lancaster, P. (1969), *Theory of Matrices*, Academic Press.

Li, H.T., Cheng, G.D. and Ruan, S.L. (2005), "Seismic response of ship lift system", *J. Dali. Univ. Technol.*, **45**, 473-479.

Liao, C.Y., Wu, Y.C., Chang, C.Y. and Ma, C.C. (2017), "Theoretical analysis based on fundamental functions of thin plate and experimental measurement for vibration characteristics of a plate coupled with liquid", *J. Sound Vibr.*, **394**, 545-574.

Liao, L.K. (2014), "Safety analysis and design of full balanced hoist vertical ship lift", *Struct. Eng. Mech.*, **49**(3), 311-327.

Michael, B. (2014), "For 75 years' ship lift of Rothensee", *Bautechnik*, **90**, 380-387.

Náprstek, J. (2015), "Combined analytical and numerical approaches in dynamic stability analyses of engineering systems", *J. Sound Vibr.*, **338**, 2-41.

Qu, W.L. and TU, J.W. (2008), "Theoretical and experimental study on seismic response control on top of three-gorges ship lift towers using magnetorheological intelligent isolation system and its key technique", *Front. Architect. Civil Eng.*, **3**(1), 32-41.

Qu, W.L., Xu, Y.L. and Lv, M.Y. (2002), "Seismic response control of large-span machinery building on top of ship lift towers using ER/MR moment controllers", *Eng. Struct.*, **24**(4), 517-527.

Ricci, R. and Pennacchi, P. (2012), "Discussion of the dynamic stability of a multi-degree-of-freedom rotor system affected by a transverse crack", *Mech. Mach. Theor.*, **58**, 82-100.

Ruan, S.L. and Cheng, G.D. (2003), "Calculation of ship-liquid-chamber coupled system in the ship lift with finite element

method in time domain", *Chin. J. Comput. Mech.*, **20**(3), 290-294.
Schinkel, E. (2001), *Schiffs Lift*, Westfälisches Industriemuseum.
Schultz, D.G. (1963), "A discussion of generalized Routh–Hurwitz conditions for non-linear systems", *Trans. AIEE Part II*, **81**(6), 377-382.
Shi, D.W., Peng, H., Zhao T.Z. and Cheng S.X. (2015), "Finite element and experimental analysis of pinion bracket-assembly of three gorges project ship lift", *J. Centr. South Univ.*, **22**(4), 1307-1309.
Shi, D.W., Shong, Z. and Liao, L.K. (2003), "Coupling analysis of ship-chamber of ship lift and parametric vibration of liquid", *Eng. J. Wuhan Univ.*, **36**, 77-80.
Song, C.S., Zhu, C.C., Liu, H.J. and Ni, G.X. (2015), "Dynamic analysis and experimental study of a marine gearbox with crossed beveled gears", *Mech. Mach. Theor.*, **92**, 17-28.
Tang, Y.Q., Chen, L.Q., Zhang, H.J. and Yang, S.P. (2013), "Stability of axially accelerating viscoelastic Timoshenko beams, recognition of longitudinally varying tensions", *Mech. Mach. Theor.*, **62**, 31-50.
Tu, J.W., Qu, W.L. and Chen, J. (2008), "An experimental study on semi-active seismic response control of a large-span building on top of ship lift towers", *J. Vibr. Contr.*, **14**(7), 1055-1074.
Weyh, B. and Kostyra, H. (1991), "Direct floquet method for stability limits determination-I: Theory", *Mech. Math. Theor.*, **26**(2), 123-131.
Weyh, B. and Kostyra, H. (1991), "Direct floquet method for stability limits determination-II: Application and phenomena", *Mech. Math. Theor.*, **26**(2), 133-144.
Wimmer, H.K. (1975), "Generalizations of theorems of Lyapunov and stein", *Lin. Algebr. Its Appl.*, **10**(2), 139-146.
Zhong, Y., Tu, J.W., Que, G., Tu, B. and Xu, J.Y. (2016), "Analysis and control of the coupled vibration between the ship lift and ship chamber", *Int. J. Civil Eng.*, **14**(5), 307-324.
Zhou, Y. (2015), "Fuzzy semi-active control and analysis of wind-induced vibration of a ship lift", *Mater. Struct.*, **48**(10), 3307-3316.

CC

Nomenclature

B	Width of the ship chamber
L	Length of the ship chamber
ρ	Density of liquid in the ship chamber
α	Angle displacement of pitching motion for the ship chamber
h	Depth of liquid in the ship chamber
θ	Angle displacement of sloshing for free surface of liquid
θ'	Angle displacement of sloshing for liquid layer with unit thickness
P	Hydrodynamic pressure in the ship chamber
F	Dynamical load of hydrodynamic and hydrostatic pressure along vertical direction at the bottom of the ship chamber
a	Distance of the lifting points
a_{cr}	Critical distance of the lifting points
m_1	Mass of the ship chamber and liquid
m_2	Mass of the gravity counterweights
H	Lifting height of the ship lift
d	Sectional diameter of the wire rope
R	Radius of the hoists and pulleys
φ_1	Angle displacement of rotation for the hoists
φ_2	Angle displacement of rotation for the pulleys
y_1	Displacements along vertical direction of the gravity counterweights m_2 in upstream
y_2	Displacements along vertical direction of the gravity counterweights m_2 in downstream
y_3	Displacement along vertical direction of the ship chamber
J_1	Equivalent moment of inertia for the hoist and torque counterweights
J_2	Equivalent moment of inertia for the pulleys
J_3	Equivalent moment of inertia for the pitching motion of the ship chamber and liquid
C	Stiffness of the synchronous shaft
K	Stiffness of the wire rope for the ship chamber
t_1	Proportion of the torque stiffness of the synchronous shaft and that of the motor drive shaft
t_2	Proportion of the stiffness of the gravity counterweights wire ropes and the stiffness of the wire rope for the ship chamber
γ_1	Damping coefficient of the torsional motion for the hoists and pulleys
γ_2	Damping coefficient of the pitching motion for the ship chamber
γ_3	Damping coefficient of the vertical motion for the ship chamber

Appendix A. Detailed expression of A_{ij} (i=1,2; j=1,2)

$$A_{11}=\begin{bmatrix} -C_1 & -C_2 & 0 & C_3 & 0 & C_4 & 0 \\ 1 & 0 & 0 & 0 & 0 & 0 & 0 \\ 0 & C_3 & -C_1 & -C_2 & 0 & -C_4 & 0 \\ 0 & 0 & 1 & 0 & 0 & 0 & 0 \\ 0 & C_5 & 0 & -C_5 & -C_6 & -C_7 & 0 \\ 0 & 0 & 0 & 0 & 1 & 0 & 0 \\ 0 & C_5 & 0 & -C_5 & -C_6 & -C_7 & 0 \end{bmatrix} \tag{A.1}$$

$$A_{12}=\begin{bmatrix} 0 & 0 & C_8 & 0 & -C_9 & 0 & 0 \\ 0 & 0 & 0 & 0 & 0 & 0 & 0 \\ 0 & 0 & C_8 & 0 & 0 & 0 & -C_9 \\ 0 & 0 & 0 & 0 & 0 & 0 & 0 \\ -C_{10} & 0 & 0 & 0 & C_{11} & 0 & -C_{11} \\ 0 & 0 & 0 & 0 & 1 & 0 & 0 \\ -C_{12} & 0 & 0 & 0 & C_{11} & 0 & -C_{11} \end{bmatrix} \tag{A.2}$$

$$A_{21}=\begin{bmatrix} 0 & 0 & 0 & 0 & 0 & 0 & 1 \\ 0 & C_{13} & 0 & C_{13} & 0 & 0 & 0 \\ 0 & 0 & 0 & 0 & 0 & 0 & 0 \\ 0 & -C_{14} & 0 & 0 & 0 & C_{15} & 0 \\ 0 & 0 & 0 & 0 & 0 & 0 & 0 \\ 0 & 0 & 0 & -C_{14} & 0 & -C_{15} & 0 \\ 0 & 0 & 0 & 0 & 0 & 0 & 0 \end{bmatrix} \tag{A.3}$$

$$A_{22}=\begin{bmatrix} 0 & 0 & 0 & 0 & 0 & 0 & 1 \\ 0 & -C_{16} & -C_{17} & 0 & 0 & 0 & 0 \\ 0 & 1 & 0 & 0 & 0 & 0 & 0 \\ 0 & 0 & 0 & -C_{18} & -C_{19} & 0 & 0 \\ 0 & 0 & 0 & 1 & 0 & 0 & 0 \\ 0 & 0 & 0 & 0 & 0 & -C_{18} & -C_{19} \\ 0 & 0 & 0 & 0 & 0 & 1 & 0 \end{bmatrix} \tag{A.4}$$

$$C_1=\frac{\gamma_1}{J_1+J_2} \tag{A.5}$$

$$C_2=\frac{K\left(R^2+t_2R^2\right)+\left(1+t_1\right)C}{J_1+J_2} \tag{A.6}$$

$$C_3=\frac{C}{J_1+J_2} \tag{A.7}$$

$$C_4=\frac{aK\left(R+t_2R\right)}{2\left(J_1+J_2\right)} \tag{A.8}$$

$$C_5=\frac{aK\left(R+t_2R\right)}{2\left(J_3+2J_s\right)} \tag{A.9}$$

$$C_6=\frac{\gamma_2}{J_3+2J_s} \tag{A.10}$$

$$C_7=\frac{a^2K\left(1+t_2\right)-2C_s}{2\left(J_3+2J_s\right)} \tag{A.11}$$

$$C_8=\frac{KR}{J_1+J_2} \tag{A.12}$$

$$C_9=\frac{t_2KR}{J_1+J_2} \tag{A.13}$$

$$C_{10}=\frac{L^2C_s-10J_sgh}{L^2\left(J_3+2J_s\right)} \tag{A.14}$$

$$C_{11}=\frac{at_2K}{2\left(J_3+2J_s\right)} \tag{A.15}$$

$$C_{12}=\frac{10\left(J_3+2J_s\right)gh+C_sL^2}{L^2\left(J_3+2J_s\right)} \tag{A.16}$$

$$C_{13}=\frac{KR}{m_1} \tag{A.17}$$

$$C_{14}=\frac{t_2KR}{m_2} \tag{A.18}$$

$$C_{15}=\frac{at_2K}{2m_2} \tag{A.19}$$

$$C_{16}=\frac{\gamma_3}{m_1} \tag{A.20}$$

$$C_{17}=\frac{2K}{m_1} \tag{A.21}$$

$$C_{18}=\frac{\gamma_3}{m_2} \tag{A.22}$$

$$C_{19}=\frac{t_2K}{m_2} \tag{A.23}$$

Appendix B. Detailed expression of b_i (i=0,1,2,⋯,14)

$$b_0 = 1 \tag{B.1}$$

$$b_1 = 2C_{10} + C_{32} + C_{53} + 2C_{62} \tag{B.2}$$

$$b_2 = C_{10}^2 + 2C_{11} + 2C_{10}C_{32} + C_{33} + C_{44} + 2C_{10}C_{53} + C_{32}C_{53} + C_{54} + 4C_{10}C_{62} + 2C_{32}C_{62} + 2C_{53}C_{62} + C_{62}^2 + 2C_{63} \tag{B.3}$$

$$b_3 = 2C_{10}C_{11} + C_{10}^2C_{32} + 2C_{11}C_{32} + 2C_{10}C_{33} + 2C_{10}C_{44} + C_{32}C_{44} + C_{32}C_{54} + C_{10}^2C_{53} + 2C_{11}C_{53} + 2C_{10}C_{32}C_{53} + C_{33}C_{53} + C_{44}C_{53} + 2C_{10}C_{54} + C_{32}C_{54} + 2C_{10}^2C_{62} + C_{10}^2C_{53} + 2C_{11}C_{53} + 2C_{10}C_{32}C_{53} + C_{33}C_{53} + C_{44}C_{53} + 2C_{10}C_{54} + 4C_{11}C_{62} + 2C_{32}C_{62} + C_{53}C_{62}^2 + 4C_{10}C_{32}C_{62} + 2C_{44}C_{62} + 4C_{10}C_{53}C_{62} + 2C_{32}C_{53}C_{62} + 2C_{54}C_{62} + 2C_{10}C_{62}^2 + C_{32}C_{62}^2 + 4C_{10}C_{63} + 2C_{32}C_{63} + 2C_{53}C_{63} + 2C_{62}C_{63} \tag{B.4}$$

$$b_4 = C_{11}^2 + 2C_{11}C_{33} + 2C_{11}C_{44} + 2C_{10}C_{11}C_{53} + 2C_{11}C_{32}C_{53} + 2C_{11}C_{54} + 4C_{10}C_{11}C_{62} + 4C_{11}C_{32}C_{62} + 4C_{11}C_{53}C_{62} + 2C_{11}C_{53}C_{62}^2 + 2C_{53}C_{62}C_{63} + 2C_{11}C_{62}^2 + 4C_{11}C_{63} + 4C_{10}C_{32}C_{63} + 2C_{33}C_{63} + 2C_{44}C_{63} + 2C_{54}C_{63} + 4C_{10}C_{53}C_{63} + 2C_{32}C_{53}C_{63} + 4C_{10}C_{62}C_{63} + 2C_{32}C_{62}C_{63} \tag{B.5}$$

$$b_5 = C_{11}^2C_{32} + 2C_{10}C_{11}C_{33} + 2C_{10}C_{11}C_{44} + 2C_{11}C_{32}C_{44} + C_{11}^2C_{53} + C_{32}C_{63}^2 + 2C_{11}C_{33}C_{53} + C_{11}^2C_{44}C_{53} + 2C_{11}C_{44}C_{53} + 2C_{11}^2C_{62} + 2C_{10}C_{11}C_{32}C_{53} + 2C_{10}C_{11}C_{54} + 2C_{11}C_{32}C_{54} + 4C_{10}C_{11}C_{32}C_{62} + 4C_{11}C_{33}C_{62} + 4C_{11}C_{44}C_{62} + 4C_{10}C_{11}C_{53}C_{62} + 4C_{11}C_{32}C_{53}C_{62} + 4C_{11}C_{54}C_{62} + 2C_{10}C_{11}C_{62}^2 + 2C_{11}C_{32}C_{62}^2 + 2C_{11}C_{53}C_{62}^2 + C_{53}C_{63}^2 + 4C_{10}C_{11}C_{63} + 4C_{11}C_{32}C_{63} + 4C_{11}C_{53}C_{63} + 4C_{11}C_{62}C_{63} + 2C_{10}C_{63}^2 \tag{B.6}$$

$$b_6 = 2C_{11}^2C_{63} + 2C_{11}C_{63}^2 + C_{10}^2C_{33}C_{54} + 2C_{11}C_{33}C_{54} + 4C_{10}C_{11}C_{44}C_{62} + 2C_{10}^2C_{32}C_{44}C_{62} + 4C_{11}C_{32}C_{44}C_{62} + 4C_{10}C_{33}C_{44}C_{62} + 2C_{11}^2C_{53}C_{62} \tag{B.7}$$

$$b_7 = 2C_{11}^2C_{32}C_{63} + 2C_{11}^2C_{53}C_{63} + 2C_{10}^2C_{44}C_{53}C_{63} + 4C_{11}C_{44}C_{53}C_{63} + 2C_{11}^2C_{62}C_{63} + 4C_{10}C_{32}C_{54}C_{63} + 4C_{10}C_{33}C_{54}C_{63} + 4C_{10}C_{44}C_{54}C_{63} + 2C_{32}C_{44}C_{54}C_{63} \tag{B.8}$$

$$b_8 = 2C_{11}^2C_{33}C_{63} + 2C_{11}^2C_{44}C_{63} + 2C_{11}^2C_{32}C_{53}C_{63} + 2C_{11}^2C_{54}C_{63} + C_{11}^2C_{63}^2 + 2C_{11}^2C_{32}C_{62}C_{63} + 4C_{11}^2C_{53}C_{62}C_{63} + 4C_{10}C_{11}C_{54}C_{62}C_{63} + 2C_{11}C_{33}C_{63}^2 + 4C_{11}C_{32}C_{54}C_{62}C_{63} + 2C_{10}C_{11}C_{32}C_{63}^2 + 2C_{11}C_{44}C_{63}^2 + 2C_{10}C_{11}C_{53}C_{63}^2 + 2C_{11}C_{32}C_{53}C_{63}^2 + 2C_{11}C_{54}C_{63}^2 \tag{B.9}$$

$$b_9 = 2C_{11}^2C_{32}C_{44}C_{63} + 2C_{11}^2C_{33}C_{53}C_{63} + 2C_{11}^2C_{44}C_{53}C_{63} + 2C_{11}^2C_{32}C_{54}C_{63} + 2C_{11}^2C_{33}C_{62}C_{63} + 2C_{11}^2C_{44}C_{62}C_{63} + 2C_{11}^2C_{32}C_{53}C_{62}C_{63} + C_{11}^2C_{53}C_{63}^2 + C_{11}^2C_{32}C_{63}^2 + 2C_{11}^2C_{54}C_{62}C_{63} + 2C_{10}C_{11}C_{32}C_{53}C_{63}^2 + 2C_{11}C_{33}C_{53}C_{63}^2 + 2C_{11}C_{44}C_{53}C_{63}^2 + 2C_{10}C_{11}C_{54}C_{63}^2 \tag{B.10}$$

$$b_{10} = 2C_{11}^2C_{34}C_{36}C_{61} - 2C_{11}^2C_{36}C_{44}C_{61} - 2C_{11}^2C_{33}C_{34}C_{63} + 2C_{11}^2C_{33}C_{44}C_{63} - 2C_{11}^2C_{32}C_{34}C_{53}C_{63} + 2C_{11}^2C_{32}C_{44}C_{53}C_{63} + 2C_{11}^2C_{44}C_{54}C_{63} - 2C_{11}^2C_{36}C_{61}C_{63} - 2C_{11}^2C_{32}C_{34}C_{62}C_{63} + 2C_{11}^2C_{32}C_{44}C_{62}C_{63} + C_{11}^2C_{33}C_{63}^2 + 2C_{11}^2C_{44}C_{53}C_{62}C_{63} + 2C_{11}^2C_{32}C_{54}C_{62}C_{63} + C_{11}^2C_{44}C_{63}^2 + C_{11}^2C_{32}C_{53}C_{63}^2 + C_{11}^2C_{54}C_{63}^2 \tag{B.11}$$

$$b_{11} = 2C_{11}^2C_{34}C_{36}C_{53}C_{61} - 2C_{11}^2C_{36}C_{44}C_{53}C_{61} + 2C_{11}^2C_{34}C_{36}C_{61}C_{62} - 2C_{11}^2C_{36}C_{44}C_{61}C_{62} + 2C_{11}^2C_{33}C_{44}C_{53}C_{63} - 2C_{11}^2C_{32}C_{54}C_{54}C_{63} - 2C_{11}^2C_{36}C_{53}C_{61}C_{63} - 2C_{11}^2C_{32}C_{34}C_{53}C_{62}C_{63} + 2C_{11}^2C_{32}C_{44}C_{53}C_{62}C_{63} - C_{11}^2C_{32}C_{34}C_{63}^2 + C_{11}^2C_{32}C_{44}C_{63}^2 + C_{11}^2C_{33}C_{53}C_{63}^2 + C_{11}^2C_{32}C_{54}C_{63}^2 + 2C_{11}^2C_{44}C_{54}C_{62}C_{63} + C_{11}^2C_{44}C_{53}C_{63}^2 + 2C_{11}^2C_{32}C_{44}C_{54}C_{63} + 2C_{11}^2C_{33}C_{54}C_{62}C_{63} \tag{B.12}$$

$$b_{12} = 2C_{11}^2C_{34}C_{36}C_{54}C_{61} - 2C_{11}^2C_{36}C_{44}C_{54}C_{61} - 2C_{11}^2C_{33}C_{34}C_{54}C_{63} + 2C_{11}^2C_{33}C_{44}C_{54}C_{63} + 2C_{11}^2C_{34}C_{36}C_{61}C_{63} - 2C_{11}^2C_{36}C_{44}C_{61}C_{63} - 2C_{11}^2C_{36}C_{54}C_{61}C_{63} + C_{11}^2C_{33}C_{44}C_{63}^2 - 2C_{11}^2C_{33}C_{34}C_{53}C_{62}C_{63} + 2C_{11}^2C_{33}C_{44}C_{53}C_{62}C_{63} - 2C_{11}^2C_{32}C_{34}C_{54}C_{62}C_{63} + C_{11}^2C_{33}C_{54}C_{63}^2 + 2C_{11}^2C_{32}C_{44}C_{54}C_{62}C_{63} - C_{11}^2C_{33}C_{34}C_{63}^2 - C_{11}^2C_{32}C_{34}C_{53}C_{63}^2 + C_{11}^2C_{32}C_{44}C_{53}C_{63}^2 \tag{B.13}$$

$$b_{13} = -2C_{11}C_{15}C_{34}C_{36}C_{53}C_{60}C_{61} + 2C_{11}C_{15}C_{36}C_{44}C_{53}C_{60}C_{61} - C_{11}^2C_{33}C_{34}C_{53}C_{63}^2 - 2C_{11}C_{15}C_{30}C_{34}C_{53}C_{61}C_{63} + 2C_{11}C_{15}C_{30}C_{44}C_{53}C_{61}C_{63} - 2C_{11}^2C_{36}C_{44}C_{53}C_{61}C_{63} + 2C_{11}^2C_{33}C_{44}C_{54}C_{62}C_{63} + 2C_{11}C_{13}C_{30}C_{34}C_{53}C_{63}^2 - 2C_{10}C_{11}C_{33}C_{34}C_{54}C_{63}^2 + 2C_{10}C_{11}C_{33}C_{44}C_{54}C_{63}^2 - C_{11}^2C_{32}C_{34}C_{54}C_{63}^2 + 2C_{11}^2C_{34}C_{36}C_{53}C_{61}C_{63} - 2C_{11}^2C_{33}C_{34}C_{54}C_{62}C_{63} - 2C_{11}C_{13}C_{30}C_{44}C_{53}C_{63}^2 + C_{11}^2C_{33}C_{44}C_{53}C_{63}^2 \tag{B.14}$$

$$b_{14} = -C_{15}^2C_{33}C_{34}C_{54}C_{60}^2 + 2C_{13}C_{15}C_{34}C_{36}C_{54}C_{60}^2 + C_{15}^2C_{33}C_{44}C_{54}C_{60}^2 - 2C_{13}C_{15}C_{36}C_{44}C_{54}C_{60} - 2C_{11}C_{15}C_{34}C_{36}C_{54}C_{60}C_{61} + 2C_{11}C_{15}C_{33}C_{34}C_{54}C_{60}C_{63} - 2C_{11}C_{13}C_{34}C_{36}C_{54}C_{60}C_{63} + 2C_{11}C_{15}C_{36}C_{44}C_{54}C_{60}C_{61} - 2C_{11}C_{15}C_{33}C_{44}C_{54}C_{60}C_{63} + 2C_{11}C_{13}C_{36}C_{44}C_{54}C_{60}C_{63} - 4C_{11}C_{14}C_{34}C_{36}C_{50}C_{61}C_{63} + 4C_{11}C_{14}C_{36}C_{44}C_{50}C_{61}C_{63} - 2C_{11}C_{15}C_{30}C_{34}C_{54}C_{61}C_{63} + 2C_{11}^2C_{34}C_{36}C_{54}C_{61}C_{63} + 2C_{11}C_{15}C_{30}C_{44}C_{54}C_{61}C_{63} - 2C_{11}^2C_{36}C_{44}C_{54}C_{61}C_{63} + 2C_{11}C_{14}C_{33}C_{34}C_{50}C_{63} + 2C_{11}C_{13}C_{30}C_{34}C_{54}C_{63}^2 - C_{15}^2C_{33}C_{34}C_{54}C_{63}^2 - 2C_{11}C_{13}C_{30}C_{44}C_{54}C_{63}^2 + C_{11}^2C_{33}C_{44}C_{54}C_{63}^2 \tag{B.15}$$